Influence of geometric parameters and image preprocessing on tomo-PIV results

Lionel Thomas, Romain Vernet, Benoit Tremblais, Laurent David

Influence of geometric parameters and image preprocessing on tomo-PIV results

L. Thomas[1], R. Vernet[1], B. Tremblais[2], L. David[1]

1: Institut Pprime, CNRS-Université de Poitiers-ENSMA, UPR3346
Département Fluides, Thermiques, Combustion
SP2MI, Bd Marie et Pierre Curie, téléport 2
86962 Futuroscope Chasseneuil, France
Lionel.Thomas@univ-poitiers.fr

2: Institut XLIM SIC, CNRS-Université de Poitiers UMR CNRS 6172
SP2MI, Bd Marie et Pierre Curie, téléport 2
86962 Futuroscope Chasseneuil, France

Abstract The tomography-PIV is using multiple camera views for a full tomographic reconstruction of the object space, which is represented by a 3-D voxel structure with a resolution adapted to the camera resolution. Influences of different parameters such as the images pre-processing, the volume discretization and the weighting matrix, the algorithm initialization and the cameras angles, the volume thickness and the particle density are studied on synthetic and real images.

1. Introduction

Tomo-PIV is a recent experimental technique originally developed by Elsinga et al (2006), which gives access to the three velocity components in a fat sheet, typically a few centimeters thick. The basic idea to get a 3D3C velocity field using tomo-PIV is to take few images of a volume containing particles, to reconstruct the light intensity distribution inside the volume and two correlate two volumes to get the most probable displacement of the particles inside the volume. The main difficulty is the reconstruction procedure, even if the correlation has to be optimized to reduce the computation time. In this paper, the attention is focused on the reconstruction step where there are still difficulties to go through. First of all, the computation time is very large. Recently, Atkinson and Soria (2009) have proposed an efficient technique to reduce the computation time, that is partially based on the work of Worth and Nickels (2008). They propose to initialize the volume by a multiplicative estimation, whereas Putze and Maas (2008) suggest using a minimum operator evaluation. Further details will be given in the following. Anyway, all these techniques are based on algebraic reconstruction methods, first introduced by Gordon et al (1970), which are slow but well adapted to the limited number of views. The MART algorithm family is still the most used for tomo-PIV. Secondly, as the problem is ill-posed, the reconstruction quality decreases as particles concentration increases. The need to add some a priori to the solution is then more and more necessary. Petra et al (2009) propose for example an alternative based on the compressed sensing theory in order to optimize the solution, but it is still theoretical.
In a first step, synthetic images are used to evaluate the influence of several parameters (that are detailed in the next section) on the reconstruction quality. In a second step, experimental images are used to study the influence of some of the previous parameters on the correlation quality. The effort is put on the discretization of the problem and on the images preprocessing influence on the reconstruction quality.

2. Methods and algorithms

The volume reconstruction is an inverse problem. The direct problem is the projection of the light intensity inside the volume onto the camera images. The projection operator is not a parallel one: its direction is a function of the position in the image and is given by the calibration procedure, which gives the geometric transformation between real and image spaces. Usually two models are used for the calibration: the Soloff polynomial model or the pinhole camera model. The later is used in this paper.

If **X**=(*X*, *Y*, *Z*) is a point in the volume, with *Z* the coordinate perpendicular to the laser sheet, and **x**=(*x*, *y*) is the corresponding point in the considered camera image, the geometric transformation and its inverse are defined respectively by equations 1 and 2.

$$x = \psi(X) \quad (1)$$

$$(X, Y) = \psi^{-1}_{(x,y)}(Z) \quad (2)$$

The set of points in space seen by a point **x** in the image is called the line-of-sight and is written *LOS*(**x**). From this, it is possible to write the projection operator on a given image (see Figure 1) and equation 3.

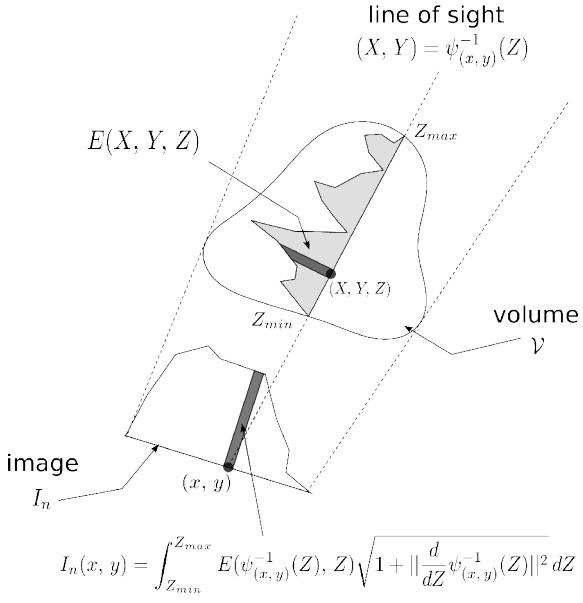

Figure 1: Definition of the projection geometry.

$$I_n(x, y) = \int_{z_{min}}^{z_{max}} E(\psi^{-1}_{(x,y)}(Z), Z)\sqrt{1 + \left\|\frac{d}{dZ}\psi^{-1}_{(x,y)}(Z)\right\|^2}\, dZ \quad (3)$$

where *I* is the image intensity, and *E* is the volume intensity. In the direct problem, *E* is known and *I* is the unknown. In the inverse problem, it is opposite.

There are several ways to solve this problem, but in the case of a limited number of views, the most used techniques are algebraic. They consist in transforming the continuous problem into a discrete one.

2.1 Problem discretization

The images are already discretized. Their size is . The pixels intensity values are stored in a vector *I*. There are two other elements to discretize: the volume and the projection operator. The volume to reconstruct is taken as the biggest volume seen by all the cameras. In this paper, and in most tomo-PIV papers, it is discretized in cubic voxels, inside which the intensity is supposed constant. Usually, the size of the voxels inside the volume is chosen such as the number of voxels along a line

is equal to the number of pixels along the projected line, but the effect of this parameter on the reconstruction is investigated in the paper. The volume dimensions is then .
With discrete images and volume, the projection operator can be written as a discrete sum (equation 4).

$$I_p = \sum_{v=0}^{N_v} w_{pv} E_v \qquad (4)$$

where *p* is the pixel considered in the image, *v* is a voxel, is the intensity at pixel *p*, is the intensity at voxel *v*, and is the interaction between the pixel *p* and the voxel *v*. Theoretically, is the intersection between a pyramid issued from the pixel contour and the voxel. In practice, it is impossible to solve the problem analytically; hence several approximations can be made. Usually, is multiplied by the voxel volume, therefore is taken as the volume fraction of the voxel intercepted by the pixel volume-of-sight.

Let's define the different approximations for the interaction studied in this paper. and are called the voxel center and the pixel center respectively.

• **direct**

If $\psi(X_v) \in pixel(p)$, then else

• **los-length**

The voxel is modeled by a sphere with a volume equal to the voxel volume. is taken as the length of the intersection between the sphere and the line-of-sight issued from the pixel center, divided by the sphere diameter.

• **raytracing**

This one is used classically in the previous tomo-PIV studies and was referenced in Lamarche and Leroy (1990). Again, the voxel is modeled by a sphere. Moreover, the pixel is assimilated to a disk, with a surface equal to the pixel size. If pixel has size 1, the diameter is $d_p = 1/\sqrt{\pi}$. As the voxel size has been chosen such as its projection has approximately the same dimensions as one pixel, the trace of the voxel projection is assimilated to a disk with diameter . is then the surface of the intersection between the two disks, divided by the surface of one disk. $d_c = \|x_p - \psi(X_v)\|$ is the distance between the two disks centers. If $d_c \geq d_p$, , else $w_{pv} = 2(a\cos(d_c/d_p) - d_c/d_p\sqrt{(1-(d_c/d_p)^2)})$

• **linear**

is computed as the weight of a linear interpolation. Let's define $\delta x = \psi(X_v) - x_p$. If $|\delta x| \geq 1$ or $|\delta y| \geq 1$, , else $w_{pv} = (1-\delta x)(1-\delta y)$

• **subpixel**

The pixel is subdivided into subpixels. is the fraction of subpixels whose line-of-sight intersect the voxel midplane.

• **subvoxel**

The voxel *v* is subdivided into subvoxels. is the fraction of subvoxels whose center is projected inside the pixel *p*.

After discretization, the problem is reduced to the inversion of a linear system. The matrix *W* is highly sparse, because on a matrix line *p*, the only non-zero values are those concerning voxels on the line-of-sight. Moreover, the problem is well-known to be ill-posed: in particular, the solution is non-unique and very sensitive to noise. So the classical least-squares method will not work properly and some specific algorithms have to be developed.

2.2 Algorithm

As only a few views are given, it is necessary to introduce some a priori on the solution, such as

regularization. In this paper, two types of regularization are used: minimization of intensity and maximization of entropy. They lead to well-known algorithms often used in tomo-PIV reconstruction. They are both iterative algorithms.
The first one is the ART algorithm (equation 5). For each pixel *p*, then for each voxel *v*:

$$E_v^{n+1} = E_v^n + \mu \frac{I_p - \sum_u w_{pu} E_u^k}{\sum_u w_{pu}^2} w_{pv} \qquad (5)$$

In this paper, a positivity constraint is added: all intensities which become negative during the iteration process are set to zero. The algorithm is then called positive ART (ART+).
The second one is the most used algorithm: the MART algorithm (equation 6). For each pixel *p*, then for each voxel *v*:

$$E_v^{n+1} = E_v^n \left(\frac{I_p}{\sum_u w_{pu} E_u^k} \right)^{\mu w_{pv}} \qquad (6)$$

This algorithm is usually preferred over ART because it is more adapted to reconstruct small contrasted objects.
In each algorithm, μ is a relaxation parameter which can be chosen between 0 and 2.

2.3 Initialization

Classically, using ART+, the volume is initialized to 0, and using MART, the volume is initialized to 1. Following Worth and Nickels (2008) the initialization of both algorithms can be made with a back projection step. There are several ways to perform this operation. For a given voxel *v*, the corresponding intensity on the image *i* is given by $E_v^{(i)} = \sum_{w_{pv} \neq 0} w_{pv} I_p^{(i)}$. These intensities can be computed using the different approximations for *W*, as defined during the discretization of the problem. The intensity of the voxel *v* can be estimated using several methods:

- **test**

if all $E_v^{(i)}$ are positive, .

- **mean if non zero**

if all $E_v^{(i)}$ are positive, $E_v = \frac{1}{N_{img}} \sum_i E_v^{(i)}$

- **product**

$E_v = (\prod_i E_v^{(i)})^{1/N_{img}}$

- **min**

$E_v = \min_i (E_v^{(i)})$

The product criteria was used by Worth and Nickels (2008) and Atkinson and Soria (2009), while the min has been used by Putze and Maas (2008).

2.4 Camera position

The cameras have been placed on one side of the volume. They are all directed towards the volume center, and they are disposed regularly on a circle. The parameter that is changed is the angle between the normal to the volume and the camera line-of-sight.

2.5 Quality evaluation

Several criteria are used to evaluate the reconstruction quality. is the projection quality. It compares the projected volume to the original images, using a normalized cross-correlation. compares also, with a normalized cross-correlation, the reconstructed volume to the volume used to make the

images. This criterion is only computable for synthetic images, when the solution is known.

3 Origin of the data

3.1 Synthetic images

The code used to compute the synthetic images and to reconstruct the volumes is developed using the C++ library (Tremblais *et al* (2010)). Synthetic images are generated by projection of synthetic volumes, using the same algorithms as for reconstruction. Here, 200×200×30 discrete volumes are used, and filled with spherical particles with gaussian intensity profile. The diameter and intensity of the particles is fixed. The particles are distributed randomly in the volume. The projection was made using the 4×4×7 subvoxel approximation for W, in order to get a good precision. The camera can be moved in all directions. The calibration pinhole matrices were generated by the projection program and used for the reconstruction. Therefore, the reconstruction problem was noiseless, and the noise influence is not studied in the present paper.

3.2 Experimental images

The final tests are made on experimental images, obtained in a hydrodynamic closed-loop channel with a 0.16 × 0.13 m² section. A pulsed jet in cross-flow for a Reynolds number ($\mathrm{Re} = \frac{U_{ref} D}{\nu}$) of 500 is recorded with four 1600 x 1200 pixels CCD JAI cameras (Vernet et al., 2009). The experimental cameras arrangement is given in Figure 2.

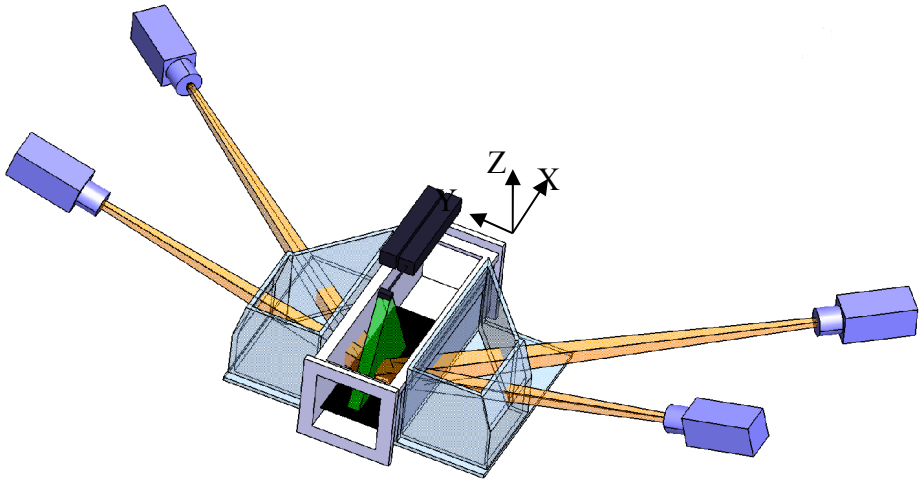

Figure 2: Cameras arrangement.

The flow is seeded with 10 µm hollow glass particles to obtain particle image density of approximately 0.02 ppp. The light source is a Quantel double-cavity Nd:YAG laser with a pulse energy of 120 mJ and is placed just above the section to be illuminated. Three laser sheet thicks (6, 25 and 30mm) have been investigated with the same particle concentration to examine the limits of seeding with the tomographic reconstruction on the experiment, and to increase the information of the flow in more than half of the interaction volume. The time between exposures is 30 ms yielding a maximum jet particle displacement of 8 pixels. Nikon objectives of 50 and 60 mm fixed focal length with an aperture of 8 and Scheimpflug adapters are mounted on each camera. They are placed on both sides of the channel and the viewing angles are approximately ±45°/Y-axis in the XY plane, ±20°/Y-axis in the YZ plane. In order to reduce the optical aberrations caused by the passage through the air–Altuglas–water dioptre (Calluaud and David, 2004), prisms filled with water are laid out against the faces of the hydrodynamic channel.
At first, a volumic calibration is applied to define the transformation between the camera references

and the object reference. A double side plate is scanned through the volume in depth direction by 5 mm step for several positions to obtain the same locations on all the cameras. For each flow exposure, the particle volume is reconstructed by applying the different preprocessing previously described. The distribution of light intensity inside discretized volumes of size varying between 767×463×125 and 1553×938×253 voxels is yielded and used to evaluate the three-dimensional displacements by 3D cross-correlation of volumes extracted at t and t+Δt. An iterative volume correlation technique returns 65×36×7 velocity vectors (for a 25mm volume width) using a final interrogation volume size of 48×48×48 voxels with 75% overlap.

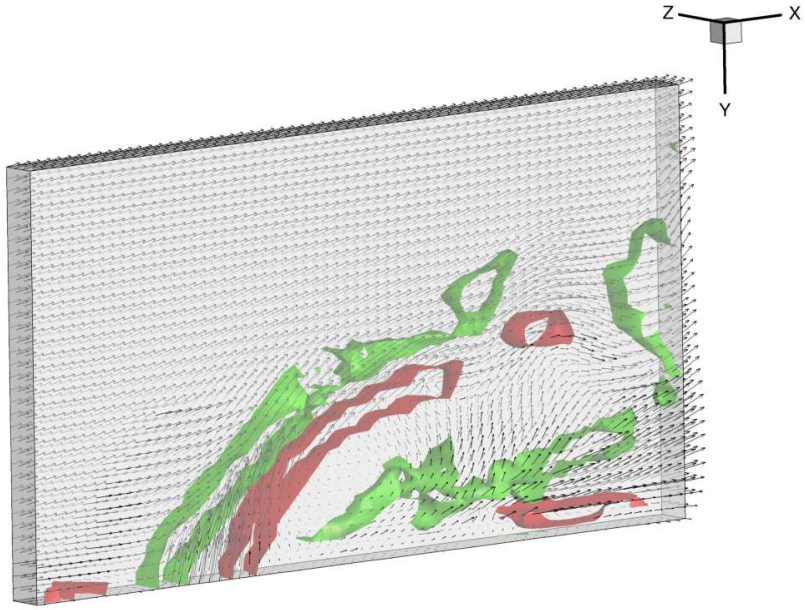

Figure 3: Velocity field and Z-vorticity iso surfaces computed with 48X48X48 windows and 75% overlap.

4. Results

4.1 Synthetic images

The first test concerns the volume discretization. The parameter studied is the ratio between the reconstructed volume voxel size and the original volume voxel size (which corresponds to a ratio pixel/voxel size equal to 1). The result is presented in . The quality of the reprojection is presented for three cases: initialization only, a single iteration and five iterations. The image projection quality decreases when the voxel size ratio is greater than one. When it is lower than one, it means oversampling. After the initialization, the quality increases with oversampling, while it becomes opposite when MART iterations number increases. In general, it is possible to conclude that voxel size ratio should be close to 1. Concerning the volume quality, it is nearly constant between 1 and 1.4, while it is much lower outside this interval. That means that it is better to slightly undersample the reconstructed volume in order to improve the volume quality, even if the reprojection quality is slightly lower.

The initialization step is the second operation in the volume reconstruction algorithm. The quality of the reconstruction is evaluated after just initialization only (Figure 5), and after 1 or 5 MART iterations (Figure 6). The initialization time is considered (Figure 7).

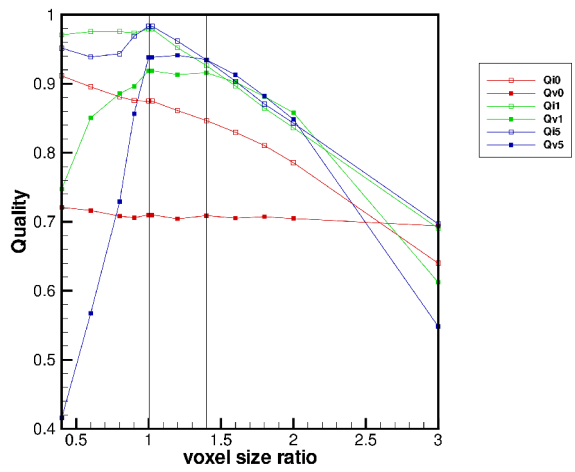

Figure 4: Comparison of the reconstruction quality variation with voxel size ratio.

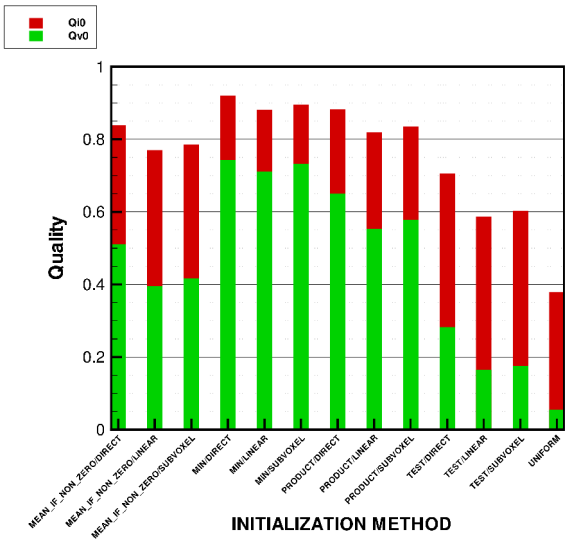

Figure 5: Comparison of the quality of the reconstruction after the backprojection operation only.

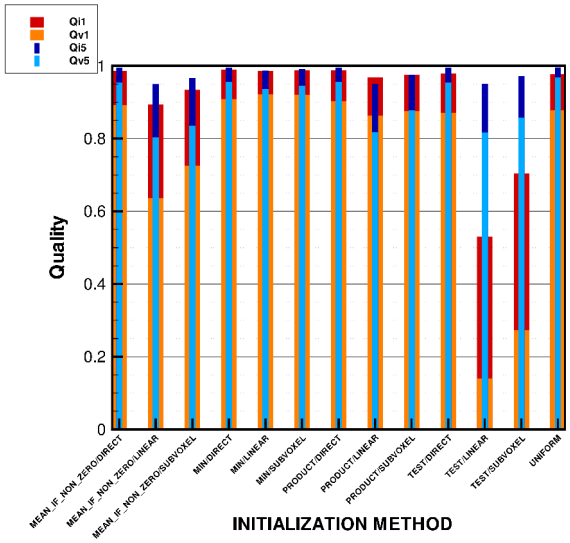

Figure 6: Comparison of the quality of the reconstruction after the backprojection operation and 5 MART iterations.

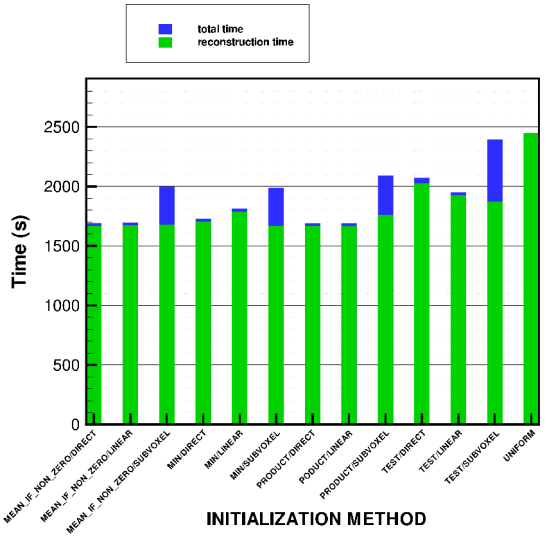

Figure 7: Comparison of the time of the reconstruction.

After 1 MART step, the min method is still the best, but min/direct, product direct and mean if non zero/direct are just slightly below min/linear and min/subvoxel. The situation is slightly different after 5 MART iterations: The uniform initialization is the best one. Very close are the couples mean-if-non-zero/direct, min/direct, product/direct, test/direct, and slightly below, min/linear and min/subvoxel. The partial conclusion is that classical MART is slightly better with 5 iterations, but when the initialization uses back projection, direct projection, and in general min method, are also better and the convergence is faster than classical MART. It is important to consider also the computation time.

After just initialization, the best back projection method for the volume quality is the min algorithm, then the product one. For the reprojection quality, it is less obvious, even if the min seems to be better. Considering the computation time, the combinations with the direct projection method are faster than the uniform initialization. But the computation time depends on the particles number when initialization is non-uniform, then for high particles density, the conclusion can be different. The results after 5 iterations for the cases min/direct and uniform are summarized in *Table 1* and *Table 2*.

The computation time gain is important for low seeding and the quality loss is weak, but for very high seeding, it is probably better to use uniform initialization.
The previous authors have used only MART, but it is interesting to compare with the ART+ algorithm. The relaxation parameter must be optimized in order to converge towards a solution, in the fastest and safest way possible. For ART+, the best relaxation parameter is always 2. Figure 8 presents the curve of the best relaxation parameter as a function of the MART step and the quality type (in red, the reprojection quality, and in green, the volume one). From this figure, it is clear that considering volume quality, the relaxation parameter should be around 1 for a few iterations, and when the number of iterations increases, the MART relaxation parameter should be decreased, as the algorithm becomes less stable. If one wants to improve the reprojection quality, the relaxation parameter should be greater (around 1.3).

	min/linear	uniform
	93.6%	96.8%
time	28min 40s	40min 47s

Table 1: Quality and computation time comparison of the min/direct and the uniform initialization methods for 1000 particles.

	min/linear	uniform
	68.4%	75.0%
time	36min 36s	40min 31s

Table 2: Quality and computation time comparison of the min/direct and the uniform initialization methods for 5000 particles.

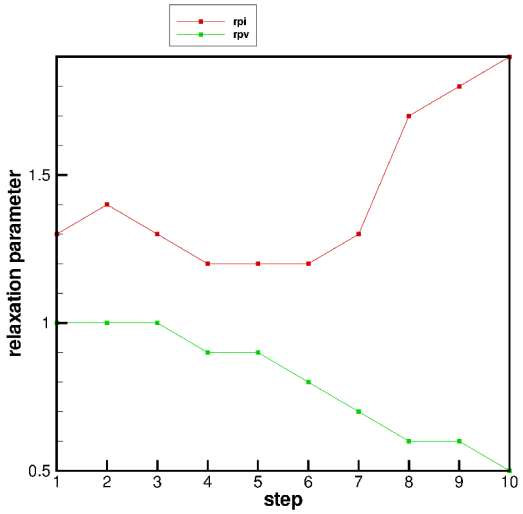

Figure 8: Best quality reconstruction relaxation parameter evolution with the number of MART steps.

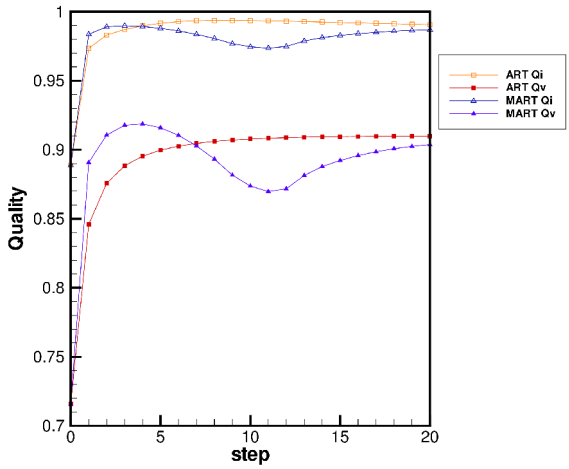

Figure 9: Comparison of ART and MART algorithms.

It is interesting to consider two representative cases to see the convergence velocity and quality. Figure 9 presents such a comparison. The ART+ relaxation parameter is equal to 2, while the MART's one is 1 to optimize volume reconstruction quality.
The ART+ algorithm converges more stably but also more slowly towards a value which is better for the reprojection quality, but worse for the volume quality. The MART algorithm is faster, but it must be stopped after a few numbers of iterations (which may vary). Otherwise, the quality oscillates and the relaxation parameter should be decreased as the step increases. In general, MART is preferred, and the iterations number never exceeds 5.

The projection parameter is an important one to study, as the initialization algorithm. The initialization is fixed to the couple min/linear. The Figure 10 and Figure 11 present the quality results after respectively 1 and 5 iterations.
After a single iteration, the result is the best for subvoxel algorithm, and it increases with the number of subvoxels. The linear algorithm is equivalent to the subvoxel 2×2×2. Subpixel 5×5 and ray tracing gives almost the same quality.
After five iterations, the tendency stays the same. Linear algorithm is equivalent to subvoxel 3×3×3 or even 4×4×2. In terms of quality, they are the ones that should be retained. It is important to consider also the computation time. It is given in Figure 12.
It is obvious that the subvoxel algorithm is very time consuming. The linear algorithm is at least twice faster (for subvoxel 3×3×3). Ray tracing is slightly faster than the linear method (30%), but as the quality is lower, the linear method is a good compromise between quality and computation time.

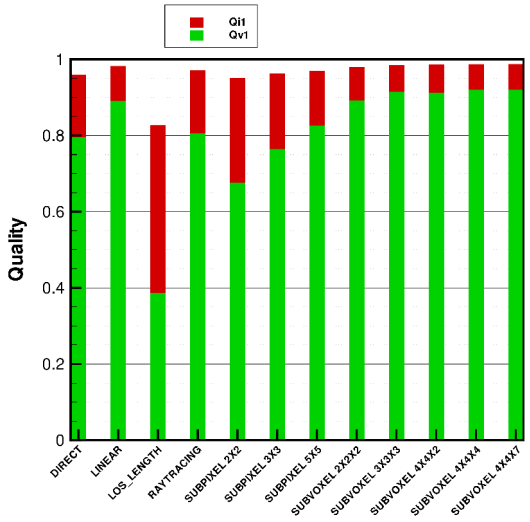

Figure 10: Comparison of the reconstruction quality variation with the projection method after 1 MART step

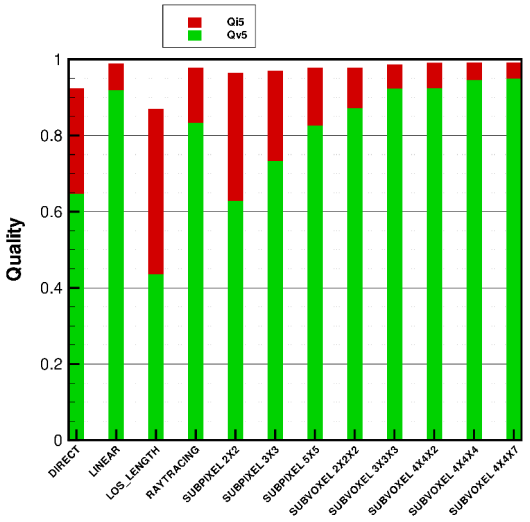

Figure 11: Comparison of the reconstruction quality variation with the projection method after 5 MART steps.

The number of cameras is also an important parameter. The Figure 13 gives the quality result for a theoretical particle density *ppp*=0.05 which a classical value. The initialization and 5 MART steps are presented. 2 up to 8 cameras views have been simulated. In general, the quality increases with the number of cameras. It is less obvious for 6 cameras, but there can be statistical errors due to the specific particles configuration. Another choice of particles could change a little bit the result. Anyway, with four cameras, the quality level for the volume is above 80% except for the initialization, therefore it is already good enough to get a good correlation.

The effect of the particles density has also been investigated in Figure 14. In this figure, three particle densities have been used: 0.025, 0.05 and 0.125. The quality increases with the cameras number. If the limit of 75% is considered, for the lowest seeding concentration, 3 cameras are enough, while for the intermediate concentration, four cameras are needed, and at least five cameras are needed for the highest concentration.

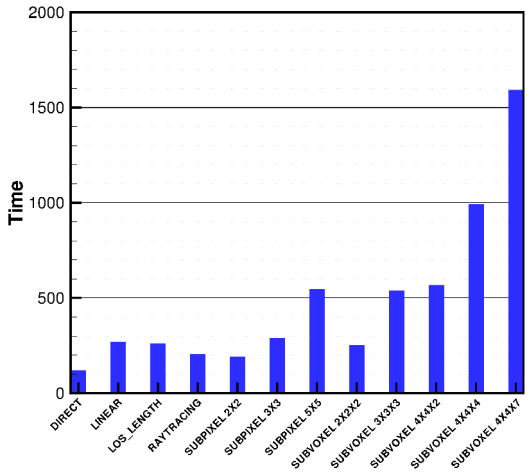

Figure 12: Comparison of the computation time variation with the projection method for 5 MART steps.

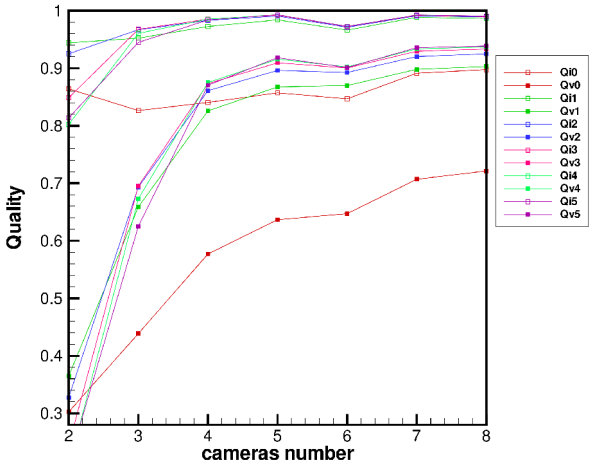

Figure 13: Comparison of the reconstruction quality variation with the camera number (with ppp=0.05).

The angle between the cameras is also varied in Figure 15. The cameras angle is the angle of each camera with the normal to the volume. From this figure, it is clear that there is an optimal angle, but there is a plateau around this value which indicates the possibility to change the camera angle approximately between 30 an 45° without changing dramatically the reconstructed volume quality. The reprojection quality is not much affected by the angle variation, except for large angles.

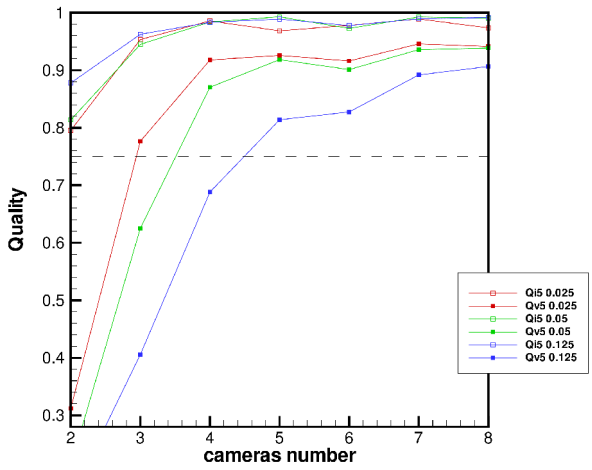

Figure 14: Comparison of the reconstruction quality variation after 5 MART iterations with the camera number (ppp=0.025, 0.05, 0.125).

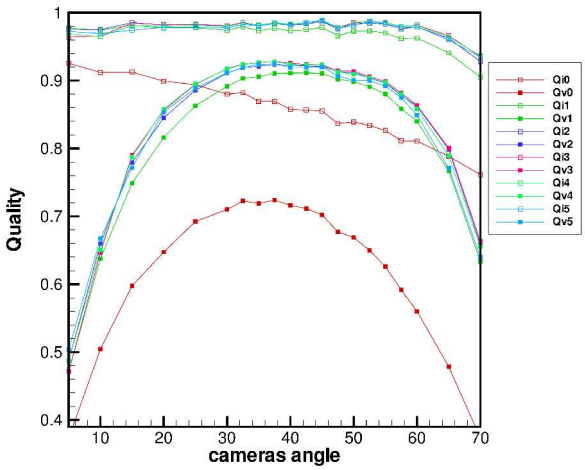

Figure 15: Comparison of the reconstruction quality variation with the cameras observation angle.

The effect of the seeding concentration on the quality has been observed previously, but it is the center of focus in Figure 16. The reconstructed volume quality is decreasing rapidly when the particles concentration is increasing. It is true at all MART step. But the reprojected quality does not change much. That means that it is not really representative of the volume reconstruction quality. The limit of 75% of is reached for a particle per voxel number *ppv*=0.0017. The theoretical *ppp* corresponding value is *ppp*=0.052.

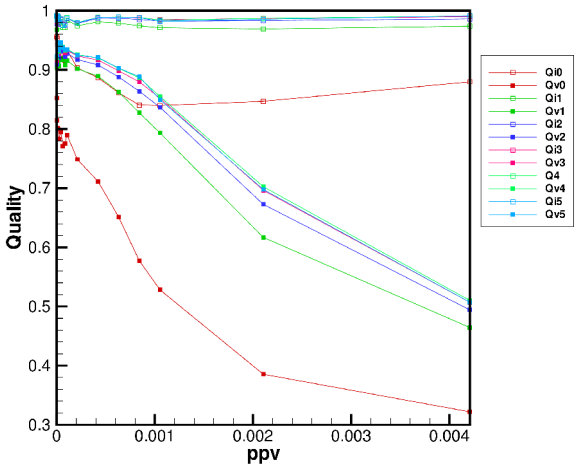

Figure 16: Comparison of the reconstruction quality variation with the particle number.

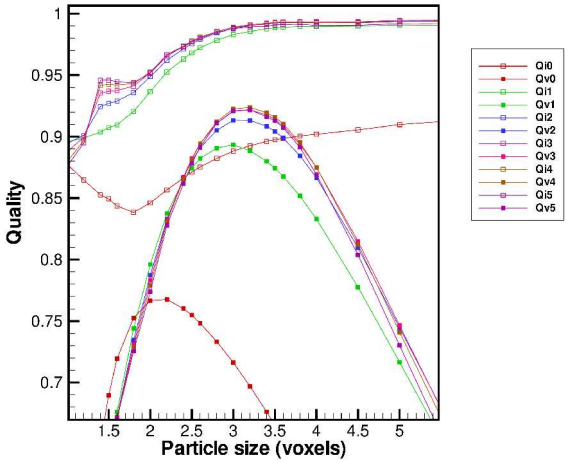

Figure 17: Comparison of the reconstruction quality variation with the particle size.

This limit is affected by the particles diameter. The Figure 17 gives the quality variation with the particles diameter. There is an optimum around 3 voxels size for the reconstructed volume quality after at least a MART step, while the optimum is around 2 for the initialization. Concerning the reprojection quality, it increases with the particles size, when is greater than 2.

4.2 Experimental images

Volumes have been computed using several different parameters and correlated with 48×48×48 windows and 75% overlap, without deformations. The *ppp* has been computed on images, because the total volume of water used during the experiment was difficult to estimate precisely. Three different volume thicknesses were used: 6mm, 25mm and 30mm. The *ppp* values were respectively estimated as 0.0182, 0.0188 and 0.0189, which means that the volume was saturated with particles. That also means that it is difficult to evaluate the particles concentration in the volume only from images. The volumes can be correlated with 32×32×32 windows for the three thicknesses. The main test has been performed on the 25mm thick measurements. Among the several reconstruction configurations studied, some of them could not lead to a correlation: reconstruction with no image preprocessing, or with too much oversampling or without initialization. The best results are obtained with a Gaussian filter in order to enlarge the particles. That can mean that the camera calibration is perfectible or that the particles are too small. The results are better when the background is eliminated by the substraction of the minimum image computed on the time series, or the average image. The main reason is probably the presence of strong reflections on the images. It seems that in this case of high particles densities, it is more important to initialize the volume than to perform many MART iterations. These conclusions should be balanced with other experiments at lower densities.

5. Conclusion

Effects of different parameters have been tested on volume reconstruction algorithms in this paper. The volume discretization has been studied. Oversampling should be limited but it is possible to slightly undersample. Different approximations of the interaction between the volume to reconstruct and the images have been studied and have shown the influence of a good projection operator discretization to increase the quality of the volume. A simple linear approximation is a good

compromise between computation speed and reconstruction quality. The volume initialization also influences the reconstruction quality. Concerning experimental results, preprocessing the images by substracting the average or the minimum grey level images improves also the quality of the reconstructed volume. But the most dramatic effect is obtained using a gaussian filter in order to enlarge the particle size. MART algorithm seems more favorable for the reconstruction. Finally, as the laser sheet thickness increases, the reconstruction quality decreases progressively but the quality seems to be acceptable for our different thicknesses, even if the limit is probably close the the thickest one.

Acknowledgements This work is funded partially by the 13th CPER and the ANR VIVE3D. Their supports are greatly acknowledged.

References

C Atkinson and J Soria. An efficient simultaneous reconstruction technique for tomographic particle image velocimetry. *Exp. in Fluids*, 47:553–568, 2009.

D Calluaud, L David. Stereoscopic Particle Image Velocimetry measurements of the flow around a surface mounted block. *Exp. in Fluids* 36(1):53-61, 2004.

GE Elsinga, F Scarano, B Wieneke, and BW van Oudheusden. Tomographic particle image velocimetry. *Exp. in Fluids*, 41:933–947, 2006.

R Gordon, R Bender, and GT Herman. Algebraic reconstruction techniques (art) for three-dimensional electron picrocopy and x-ray photography. *J. Theor. Biol.*, 29:471, 1970.

F Lamarche and C Leroy. Evaluation of the volume of intersection of a sphere with a cylinder by elliptic integrals. *Comput. Phys. Commun.*, 59:359–369, 1990.

S Petra, A Schröder, and C Schnörr. *3D Tomography from Few Projections in Experimental Fluid Dynamics*, pages 63–72. Springer, 2009.

T Putze and HG Maas. 3d determination of very dense particle velocity fields by tomographic reconstruction from four cameras views and voxel space tracking. In *ISPRS congress, Vol XXXVII part B5 Commission V*, pages 33–38, Beijing, 2008.

B Tremblais, L David, D Arrivault, J Dombre, L. Chatellier and L Thomas. SLIP: Simple Library for Image Processing (Version 1.0), http://www.sic.sp2mi.univ-poitiers.fr/slip/, Université de Poitiers, France}, 2010.

R Vernet, L.Thomas, P. Braud, L.David. Time-resolved simultaneous SPIV-PLIF and orthogonal PLIF measurements in a pulsed jet in crossflow. *8th International Symposium on Particle Image Velocimetry*, Melbourne, Victoria, Australia, August 25-28, 2009

NA Worth and TB Nickels. Acceleration of tomo-piv by estimating the initial volume intensity distribution. *Exp. in Fluids*, 45(5):847–856, 2008.